

Identification of linear and nonlinear propagation regimes in an optical fiber link using chaos analysis

Rony Rahamim

Uri Mahlab

ECI Telecom
Network Solutions Division
30 Hasivim Street
Petach Tikva 49517
Israel

and

Holon Institute of Technology
Electrical Engineering Department
Holon, 58102
Israel

David Dahan

ECI Telecom
Network Solutions Division
30 Hasivim Street
Petach Tikva 49517
Israel
E-mail: david.dahan@ecitele.com

Abstract. We propose and demonstrate a novel approach to identify linear and nonlinear propagation regimes of an optical signal in an optical fiber link by using chaos analysis. We show that the chaotic characteristics of a propagating optical signal are affected by both the chromatic dispersion and the nonlinear effects in the optical fiber. Linear or nonlinear behavior is detected by determining the maximum Lyapunov exponent of the signal and the use of the recurrence plot technique. An experimental demonstration is performed using 10-Gbps signal propagation in a 100-km fiber link with different launched optical powers. Chaos analysis shows a clear identification of the linear and nonlinear optical propagation regimes by using a classification scheme based on a multilayer neural network. Numerical simulations confirm the experimental results. © 2009 Society of Photo-Optical Instrumentation Engineers. [DOI: 10.1117/1.3247130]

Subject terms: chaos; optical communication; nonlinear optics; signal processing.

Paper 090184R received Mar. 17, 2009; revised manuscript received Jun. 28, 2009; accepted for publication Aug. 10, 2009; published online Oct. 12, 2009.

1 Introduction

Deployment of high-speed transparent and reconfigurable optical networks requires effective flexible and robust optical performance-monitoring (OPM) techniques¹ to ensure high-quality service. Indeed, these networks are susceptible to various types of impairments, which may vary over the time. Knowledge of signal degradation can therefore be used to identify the signal impairment cause and its location. This can also provide different mitigation schemes such as impairment compensation or traffic rerouting over another network segment. One of the most crucial impairments in optical networks is fiber nonlinearity, which leads to severe power-dependent degradation of the signal quality, especially at bit rates of 10 Gbps and beyond, and is one of the most difficult parameters to monitor. Therefore, it is necessary to develop robust and effective OPM techniques capable of identifying the nonlinear operation regime in the network. From a maintenance point of view, it is critical for the service provider to identify physical nonlinear impairments accumulated along the light path via the placement of OPM elements¹ at different location in the optical network.

In today's deployed networks, optical power monitoring is the common method to detect a possible nonlinear propagation regime. However, in reconfigurable mesh optical networks where dynamic equalization elements are used, remote optical power monitoring is not an effective prediction method since the link power budget can change dynamically. Indeed, the signal could undergo a nonlinear regime propagation in a section of the link due to an unex-

pected increase of its optical power (caused by some amplifier transient effects, for example). However, since the signal optical power is dynamically equalized when passing through a reconfigurable add-drop multiplexer (ROADM), it is not possible to detect the signal nonlinear propagation using power monitoring at a fiber section located after the ROADM.

It is required that the detection of the nonlinear behavior should also be possible at remote locations, which are far away from the fiber section, where the nonlinear effects take place. Several approaches have been proposed in the literature recently. For example, in Ref. 2, the authors propose a new paradigm for determining nonlinear physical impairments using Q factor estimation based on the choice of few cumulative criteria (residual dispersion and nonlinear average phase variation). Wu et al.³ proposed a technique using artificial neural networks based on eye diagram and eye histogram parameters to monitor several impairments, and among them, the signal nonlinearity strength.

Here, we propose a novel approach to determine the signal propagation regime, based on chaos theory, a branch of nonlinear analysis, which is used to describe nonrepeating systems that are too complex for traditional techniques.

Detailed theoretical and experimental investigations of semiconductor laser dynamics have shown chaotic behaviors⁴ and have paved the way to optical chaotic communication.⁴⁻⁶ Furthermore, conventional optical communications are based on semiconductor lasers as optical sources. While propagating in optical fiber, the optical signals might undergo nonlinear effects such as self-phase modulation (SPM), cross-phase modulation (XPM), four-wave mixing (FWM), stimulated Brillouin scattering

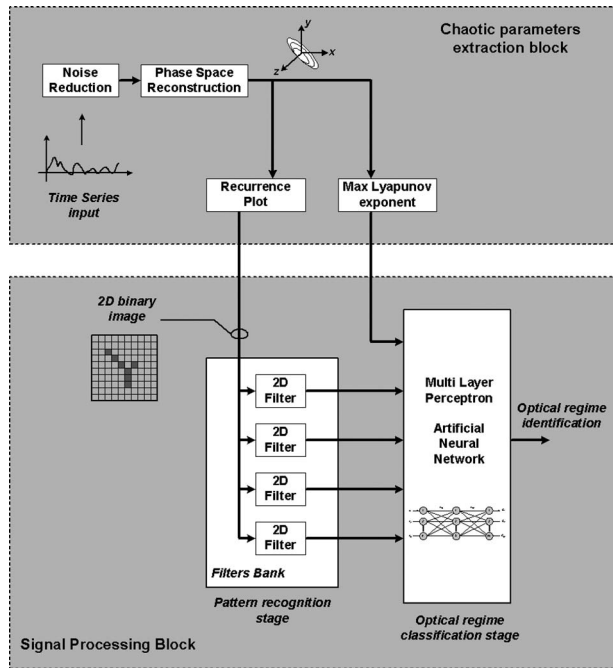


Fig. 1 Optical propagation regime identification scheme.

(SBS), and stimulated Raman scattering (SRS), which might affect the chaotic properties of the propagating optical signals. Therefore, chaos and time-series analysis seem naturally applicable to identify nonlinearity in optical network systems.

In this paper, the chaos theory is used to identify linear and nonlinear propagation regimes of a single channel in an optical link. Therefore, we focus our analysis on the interaction between chromatic dispersion (CD), SPM, and SBS only. This paper is organized as follows. Section 2 provides the principles of the proposed approach using the chaos theory. Section 3 describes the experimental setup used with a 10-Gbps signal launched into a 100-km-long fiber. In Sec. 4, the different optical propagation regimes are defined. Experimental and numerical results are presented and discussed. In Sec. 5, the chaos and time-series analysis is presented. The maximum Lyapunov exponent (MLE) and the recurrence plot (RP) derived from the phase space of the signal are calculated from experimental and numerical results. The impact of the chromatic dispersion and the optical power is discussed. The signal processing approach for

optical propagation regime identification is described and discussed in Sec. 6. After the conclusion, in Sec. 7, an appendix is provided in Sec. 8 to briefly introduce the different steps used in the chaos theory comprising the concepts of time series, phase space reconstruction, Lyapunov exponent, and RP calculations.

2 Principles of the Optical Propagation Regime Identification

The proposed approach to identify the optical propagation regime of an optical signal is presented in the block diagram of Fig. 1, which is composed by two main subblocks.

The first subblock refers to the chaotic parameter extraction block. This subblock derives the different chaotic parameters from the detected optical signal. First, the phase space of the optical time-series signal^{7,8} is reconstructed after having removed its noise component in the noise-removing stage. The attractor founded from the phase space reconstruction is used to derive the MLE (Ref. 9) and the RP (Ref. 10). The MLE provides a direct measure of the sensitive dependence on initial conditions by quantifying the exponential rates at which neighboring orbits on an attractor diverge (or converge) as the system evolves in time. The RP provides, for a given moment, the times at which a phase space trajectory visits roughly the same area in the phase space. Each of the previous steps is described with more details in Sec. 8.

The second subblock refers to the signal-processing block, where the extracted chaotic parameters are processed to identify the optical propagation regime of the detected signal. The RP matrices are treated as 2-D binary images. They are used as the input to the pattern-recognition-processing block. There are many well-know mature techniques for pattern recognition.^{11,12} In this analysis, matched filters, known as phase-only filters¹³ (POFs) are implemented and provide good discrimination capabilities. A training set of optical signals with different optical power levels provides different nonlinearity degrees and serves to design the POFs for the filter bank. These filters are used to classify the nonlinearity level by cross-correlation with the constructed RP of the signal whose optical launched power is to be determined. In the last step, the calculated MLE value is combined to the output cross-correlation results as inputs to a multilayer perceptron neural network, which provides an identification of the nonlinearity strength of the tested optical signal.

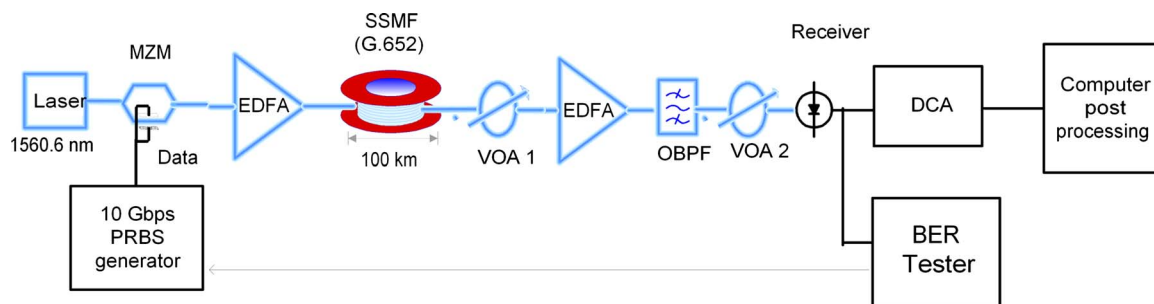


Fig. 2 Optical network test setup.

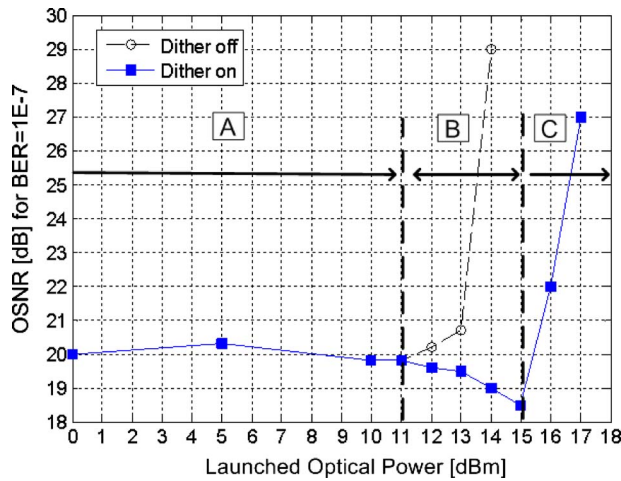


Fig. 3 Measured OSNR dependence on optical launched power for $\text{BER}=1 \times 10^{-7}$ in the case of a 10-Gbps signal with and without amplitude dither. The different optical propagation regimes regions (A, B, and C) are indicated.

3 Experimental Setup

Figure 2 shows the experimental setup used to evaluate the optical propagation regime of an optical signal launched into a standard single-mode fiber (SSMF) [International Telecommunication Union (ITU) standard G.652]. An optical Mach-Zender modulator (MZM) modulates a cw beam produced by a semiconductor laser at 1560.6 nm with a pseudo random binary signal (PRBS) at a bit rate of 10 Gbps. To increase the SBS threshold, an amplitude dither of 10 kHz is applied to the optical signal with a modulation depth of 5%. An erbium doped fiber amplifier (EDFA) is used to provide several optical launched power levels, to stimulate different levels of SPM and SBS in 100 km of SSMF. At the link end, the optical signal is amplified, filtered using an optical band pass filter (OBPF) to remove the amplifier noise and then detected. A variable optical attenuator (VOA) is placed before the second EDFA to control the optical signal-to-noise ratio (OSNR) for bit error rate (BER) measurements. The optical received power is kept constant using a second VOA. The detected optical signal is sampled using a digital communication analyzer (DCA) to produce the optical discrete time-series data to be analyzed according to the chaos theory. Each unit of sampled data contains a pattern of 512 bits with eight samples per bit and is postprocessed using the chaos-based optical propagation regime identification algorithm. In the experiment, launched optical power levels of 5, 10, 12, 14, and 16 dBm are used.

Numerical simulations of the signal propagation are also performed using the split step Fourier method algorithm.¹⁴ The nonlinear propagation regime identification algorithm is then also applied to the simulated detected signal to be compared to the experimental results.

4 Optical Propagation Regimes

OSNR dependence on the launched optical power is measured to determine the different propagation regimes of the signal. The OSNR is measured over a bandwidth of 0.1 nm to reach a reference BER of 1×10^{-7} . Figure 3 shows the

dependence of the measured OSNR with respect to the optical launched power. According to the graph, three different optical propagation regimes can be characterized for the launched optical power:

1. *Linear propagation regime (regime A, up to 11 dBm):* The required OSNR is almost constant and independent of the launched power. Fiber nonlinearities are negligible.
2. *Medium nonlinear propagation regime (regime B, from 11 to 15 dBm):* The required OSNR decreases with the launched power because of the eye-opening enhancement of the detected signal due to the interaction between chromatic dispersion and SPM.
3. *High nonlinear propagation regime (regime C, higher than 15 dBm):* the required OSNR increases exponentially because of the strong signal distortion induced by SBS and the enhanced strength of SPM.

The SBS threshold is measured to be around 15 dBm. The high SBS threshold is obtained via amplitude dithering of the signal. Without optical dithering the SBS threshold is found to be 12 dBm, as shown in Fig 3.

5 Chaos and Time-Series Analysis

5.1 Chaotic Parameter Extraction

For each time-series data sample (the sampled detected optical signal), the phase space attractor is reconstructed after noise reduction process step.

The phase space of the optical system can be reconstructed from a single scalar time series $x(t)$, $t=1, 2, \dots, N$ of the sampled optical signal by using the delay-embedding theorem.⁸ This theorem states that an appropriate phase space can be reconstructed using only the original time series and its time-delayed copies expressed as

$$\mathbf{X}_i = \{x_i, x_{i+\tau}, x_{i+2\tau}, \dots, x_{i+(m-1)\tau}\} \quad i = 1, 2, \dots, L, \quad (1)$$

where \mathbf{X}_i is the m -dimensional state vector (known also as the attractor⁸), x_i is the original sampled detected optical signal, τ is the time delay between copies, and m is the embedding dimension. Appropriate values for τ and m can be obtained using several methods.^{15,16} The delay-embedding dimension is found using the False Nearest Neighbors (FNN) procedure¹⁵ and its optimal value is found to be $m=3$. The optimal value for the time delay is found to be $\tau=3$ by using the average mutual information (AMI) approach.¹⁵

Figure 4 shows the reconstructed attractor from the back-to-back detected sampled signal. The attractor exhibits its complex trajectories, which clearly show that the optical signal has inherently chaotic characteristics due to the nonlinear complex dynamic of the semiconductor diode laser.

The reconstructed attractors for both the experimental and numerical signals are shown in Fig. 5 for the cases of launched power of 5, 10, 14, and 16 dBm and show good agreement. A multimedia animation (Video 1) is provided for the simulated optical signal. The pattern obtained from the experimental sample launched optical signal is used as the input optical data pattern for the simulation of the fiber propagation to provide a common initial attractor for adequate comparison with the experimental results. Both at-

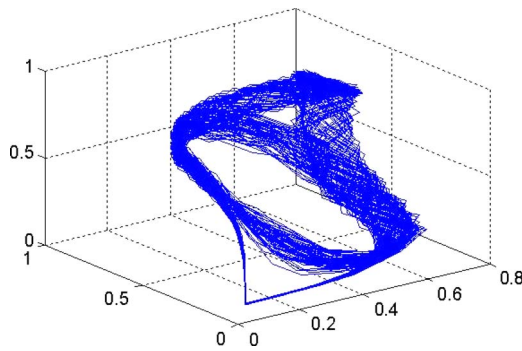


Fig. 4 Reconstructed attractors for the experimental back to back 10 Gbps signal.

tractors evolve in a similar manner when the launched optical power level is increased. In both cases, the hole in the left-hand lower corner becomes closed when the optical power increases, while the attractor broadens and becomes more distorted.

The MLE is calculated by applying the method described in Appendix A.3. Figure 6 shows the calculated MLE (extracted from the reconstructed attractor) as a function of the launched optical power after propagation into 100 km of optical fiber, corresponding to an accumulated chromatic dispersion of 1650 ps/nm. Both experimental and numerical results exhibit very good agreement with a relative error less than 2.5%. The experimental results (shown as square dots) are obtained by averaging the MLE values based on the analysis of 50 different time series of the detected signal.

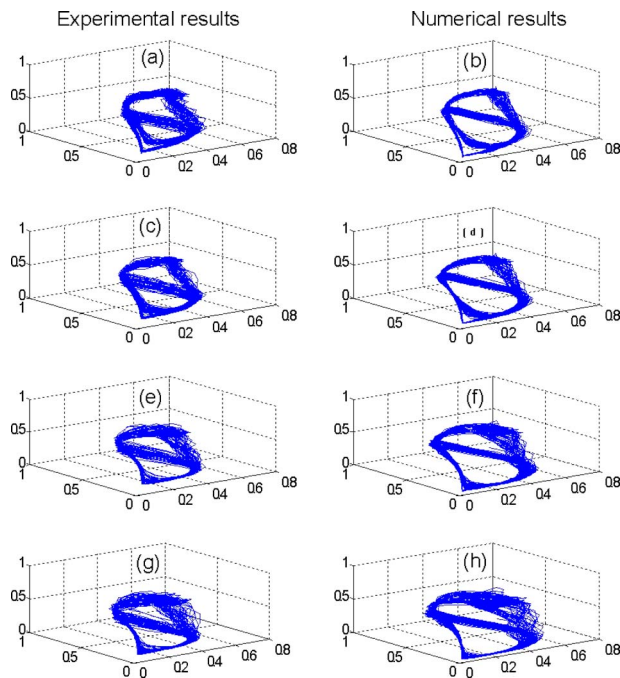
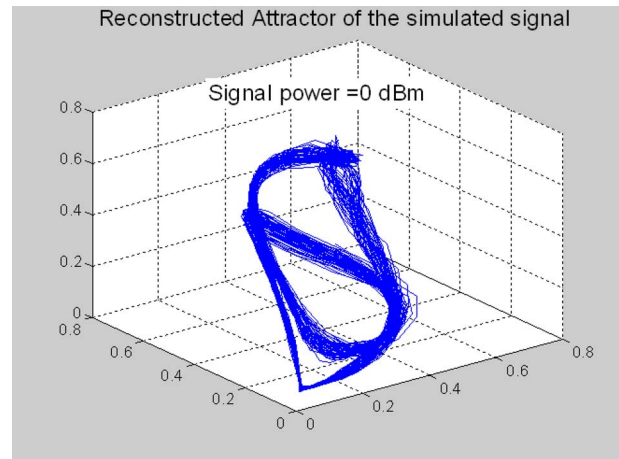


Fig. 5 Reconstructed attractors for both the experimental and numerical results (Video 1) in the case of a 10-Gbps signal with launched power of (a) and (b) 5 dBm, (c) and (d) 10 dBm, (e) and (f) 14 dBm, and (g) and (h) 16 dBm.



Video 1 Evolution of reconstructed attractors derived from numerical results in the case of 10-Gbps signal with launched power from 0 to 16 dBm (MPEG, 1.6 MB). [URL: <http://dx.doi.org/10.1117/1.3247130.1>].

The three optical propagation regimes (A, B, and C), defined previously, are also easily identified. In the linear propagation regime (A), the MLE increases slowly with the launched optical power, while in the medium nonlinear regime (B), the MLE increasing rate is dramatically enhanced. In the high nonlinear propagation regime (C), the MLE decreases. The MLE decreasing rate is also affected by the SBS effect, whose threshold was measured to be around 15 dBm. Numerical calculations were also performed in the case where the SBS effect is not taken into account and show a higher decreasing rate. Indeed, the SBS effect acts as a power limiter in the optical fiber by back-reflecting the exceeding optical launched power during the first few kilometers of the propagation. Therefore, the SBS reduces the SPM strength, leading to a softening of the MLE decreasing rate.

Since the MLE exhibits a nonmonotonic behavior, the optical propagation regime identification cannot be based

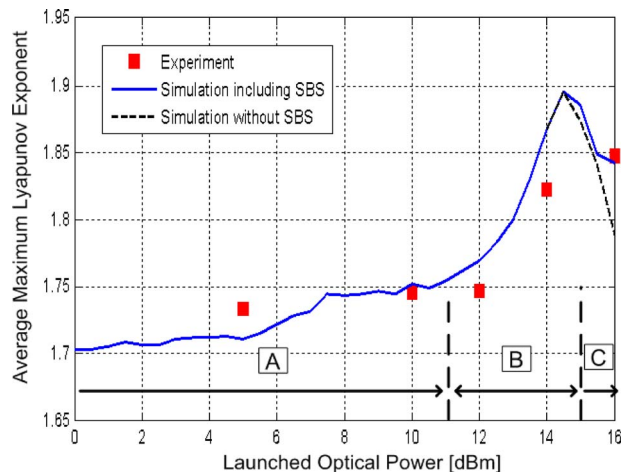


Fig. 6 MLE of the 10 Gbps after propagating into 100 km of SSMF as a function of the launched optical power; experimental and simulation results. The three propagation regimes regions (A, B, and C) are indicated.

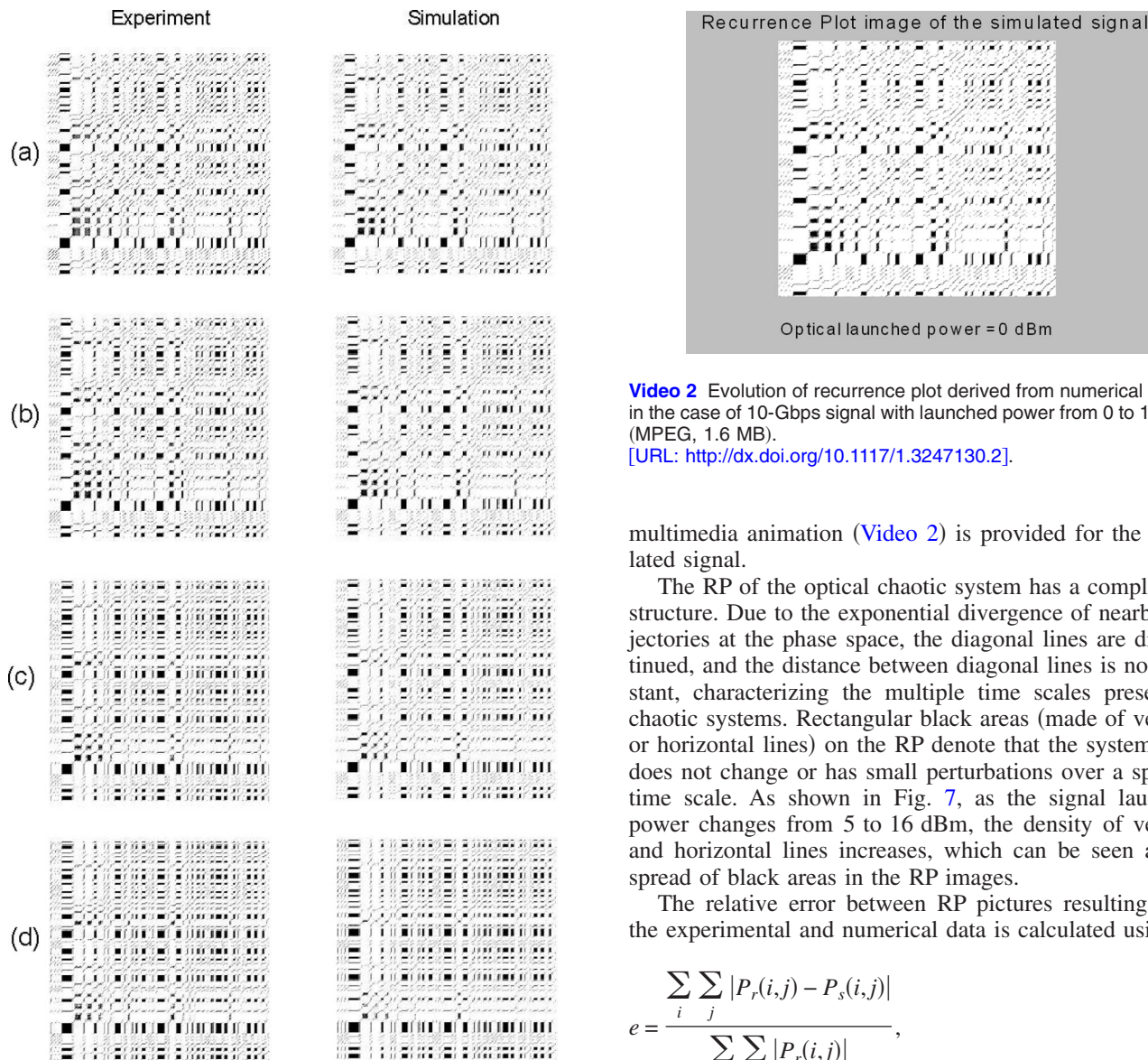


Fig. 7 RP (1024 × 1024 pixels) of the experimental and numerical 10 Gbps signal (Video 2) for launched powers of (a) 5, (b) 10, (c) 14, and (d) 16 dBm.

only on this parameter since it can lead to an ambiguity. Therefore, the RP extracted from the phase space of the optical sampled signal is used to strengthen the estimation precision. The RP of each attractor is calculated with a cutoff distance of $\varepsilon=0.005$ (see Appendix A.4). The RP presents a recurrent pattern structure, which is shown in Fig. 7 in both cases of the experimental and numerical results for launched powers of 5, 12, 14, and 16 dBm. A

Video 2 Evolution of recurrence plot derived from numerical results in the case of 10-Gbps signal with launched power from 0 to 16 dBm (MPEG, 1.6 MB).
[URL: <http://dx.doi.org/10.1117/1.3247130.2>].

multimedia animation (Video 2) is provided for the simulated signal.

The RP of the optical chaotic system has a complicated structure. Due to the exponential divergence of nearby trajectories at the phase space, the diagonal lines are discontinued, and the distance between diagonal lines is not constant, characterizing the multiple time scales present in chaotic systems. Rectangular black areas (made of vertical or horizontal lines) on the RP denote that the system state does not change or has small perturbations over a specific time scale. As shown in Fig. 7, as the signal launched power changes from 5 to 16 dBm, the density of vertical and horizontal lines increases, which can be seen as the spread of black areas in the RP images.

The relative error between RP pictures resulting from the experimental and numerical data is calculated using

$$e = \frac{\sum_i \sum_j |P_r(i,j) - P_s(i,j)|}{\sum_i \sum_j |P_r(i,j)|}, \quad (2)$$

where $P_r(i,j)$ and $P_s(i,j)$ are the RP binary pictures derived from the experiment and the simulation, respectively, for identical launched power levels.

As shown in Table 1, the error is less than 5.1% for launched power levels between 5 and 16 dBm. This indicates a good agreement between the RP images obtained and both the experiment and the simulation.

5.2 Impact of Chromatic Dispersion and Optical Power

Besides the impact of nonlinear effects, optical signals are also affected by chromatic dispersion, which leads to tem-

Table 1 Normalized error between the RPs obtained with the experimental and numerical signals as a function of the optical launched power in the case of a 10 Gbps signal propagating in 100 km of SSMF.

Launched Power	5 dBm	10 dBm	12 dBm	14 dBm	16 dBm
Relative error (%)	4.52	4.79	5.1	4.9	4.67

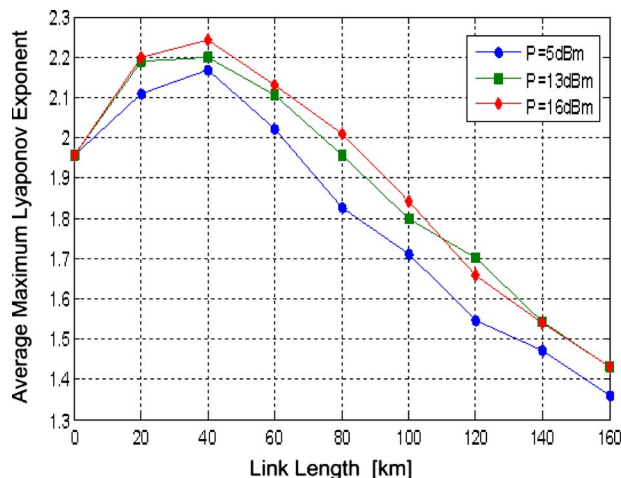


Fig. 8 Numerical dependence of the MLE on the 10-Gbps signal on the fiber length for three launched power levels (5, 13, and 16 dBm) in the SSMF.

poral signal distortions. Therefore, it is expected to have an influence on the chaotic parameters of the signal. Figure 8 shows numerical simulations of the evolution of the calculated average MLE value for a 10-Gbps signal as a function of the link length of the SSMF (and therefore as function of different accumulated dispersion levels). Three launched power levels (5, 13, and 16 dBm) corresponding to the three signal propagation regimes as defined previously in Fig. 3 (A, B, and C), are considered. Figure 8 shows that the average MLE value exhibits a similar behavior for the three launched power levels with an increasing slope up to 40 km of SSMF followed by a decreasing slope to 160 km of SSMF. The average MLE level is therefore affected by the combination of chromatic dispersion and nonlinear effects while keeping the same tendencies for the different launched powers.

In an optical network, the propagation length is not fixed. However, the residual dispersion is designed and limited to a specific range to provide optimum transmission performance. Therefore, we investigated numerically the dependence of the average MLE on the link length (from 100 to 160 km) while keeping the residual dispersion level constant (1650 ps/nm), as shown in Fig. 9. The same residual chromatic dispersion level is achieved by adding dispersion-compensating fiber (DCF) at the link end. The influence of the link length is analyzed for the three launched power levels (5, 13, and 16 dBm) in the SSMF, as defined previously. Two input power levels (−10 and 0 dBm) into the DCF are considered. For an input power of −10 dBm into the DCF, the average MLE value exhibits no dependence on the link length and for each launched power in the SSMF, it shows an equivalent behavior to the specific case of the fiber link of 100 km. Indeed, the nonlinear effects takes place only in the first few kilometers of the link corresponding to the effective fiber length¹⁴ ($L_{\text{eff}} = 14.4$ km), while chromatic dispersion is the only dominant effect afterward. Therefore, the DCF compensates the link dispersion at a level making the link equivalent to a 100-km link. When the input power to the DCF is increased to 0 dBm, the average MLE curves are identical to those of

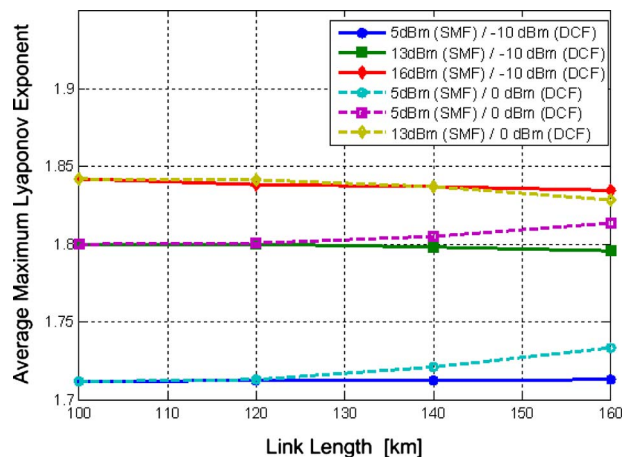


Fig. 9 Numerical dependence of the MLE on the 10-Gbps signal on the fiber length for three launched power levels (5, 13, and 16 dBm) in the SSMF assuming a constant residual chromatic dispersion of 1650 ps/nm.

the previous case (−10 dBm) for link lengths up to 120 km but show some deviations for higher link lengths. Indeed, an increase of the MLE level is obtained for launched powers of 5 and 13 dBm, while a decrease of the MLE level is obtained for launched power of 16 dBm. These deviations at the three different launched power levels suggest that the nonlinear level of the signal increases while propagating in the DCF. Indeed, when increasing the link length, the DCF length increases also to compensate the excess of chromatic dispersion. DCFs exhibit higher nonlinear coefficients than SSMF and nonlinear effects accumulate with the increase of DCF length and input power into the DCF.

These simulations demonstrate that the chaotic parameters of the detected signal are affected by both the chromatic dispersion and the nonlinear effects. Furthermore, it shows that chaos and time-series analysis is not focused on the study of a specific link configuration only but provides consistent results for a broad class of link configurations having the same residual chromatic dispersion level as long as we follow the network design rules and prevent the DCFs from increasing of the signal nonlinear regime.

6 Propagation Regime Identification Algorithm

The procedure to identify the optical propagation regime is composed by the following two stages:

1. *Pattern recognition stage*: This involves cross-correlation between the RP derived from the phase diagram of the optical signal and a bank of predefined POFs.
2. *Optical regime classification stage*: Identification of the optical propagation regime in this stage is based on a classification algorithm using an artificial neural network approach.

We demonstrated the identification algorithm performances with the experimental time-series data collected from the transmission of a 10-Gbps signal in a 100-km SSMF link.

Table 2 Statistics of the maximum cross-correlation results of different experimental signals with the POF bank in the case of a 10-Gbps signal propagating in 100-km of SSMF.

Signal Power	POF Bank									
	5 dBm		10 dBm		12 dBm		14 dBm		16 dBm	
	Mean	Std.	Mean	Std.	Mean	Std.	Mean	Std.	Mean	Std.
5 dBm	1.00	0.00	0.76	0.05	0.76	0.07	0.66	0.05	0.66	0.04
10 dBm	0.85	0.06	0.99	0.02	0.93	0.06	0.85	0.04	0.82	0.04
12 dBm	0.78	0.07	0.91	0.07	0.99	0.02	0.91	0.06	0.90	0.06
14 dBm	0.66	0.07	0.78	0.11	0.79	0.11	0.99	0.03	0.95	0.05
16 dBm	0.64	0.03	0.73	0.03	0.77	0.04	0.97	0.04	0.99	0.03

6.1 Pattern Recognition Stage

From the RP images of a training set of time-series data samples with known optical launched power, a POF bank was constructed to be cross-correlated with the RP extracted from the time-series optical signals with unknown launched power levels. The bank filter providing the cross-correlation result with the maximum peak value provides an estimation of the optical launched power level of the signal.

Table 2 shows the normalized maximum peak statistics of the cross-correlation results for a set of several time-series samples with the different POFs from the bank for the case of a 100-km transmission link. The average value (mean) and the standard deviation (std.) of the cross-correlation are given for each POF in the filter bank. The table shows that the cross-correlation procedure enables us to estimate the level of the launched signal power and therefore provides an estimation the optical propagation regime into the fiber. For the maximum cross-correlation value, nonzero standard deviation values indicates that the launched power levels of some data series samples are incorrectly identified. When used as a stand-alone step for optical propagation regime identification, it has been found that a statistics over a set of 20 time-series samples is enough to correctly determine the launched signal power level and therefore the optical propagation regime.

To increase the estimation accuracy, we combine this step with a classification stage based on artificial neural network.

6.2 Optical Regime Classification Stage

The cross-correlation results derived from pattern recognition stage and the calculated MLE value are used to identify the launched optical power and therefore the linear or nonlinear propagation regimes. The motivation for using a neural network as a classification scheme is the significant reduction of the number of time-series data samples required for a decision. Furthermore, combining the MLE with the cross-correlation results increases the algorithm accuracy.

Although many neural network architectures and connection topologies exist, the proposed approach uses the multilayered architecture called the multilayer perceptron

and the generalized structure called the nonrecurrent feed-forward.¹⁷ Multilayer neural networks solve the classification problem for nonlinear sets by employing hidden layers, whose neurons are not directly connected to the output. The additional hidden layers can be interpreted geometrically as additional hyperplanes, which enhance the separation capacity of the network. The classification problem is treated as a supervised training problem, where in the training process, the network learns to correctly classify a training set of known vectors.

A multilayer perceptron consisting of only two layers was used. In the hidden layer 30 neurons were used, while the output layer was composed by 5 neurons since there are five classes, noted 1 to 5, each one for a launched optical power level (5, 10, 12, 14, and 16 dBm, respectively).

The vectors input to the neural network consisted of the six elements: the first five elements are the maximum peak values of cross-correlation results between the RP and predefined POF and the last element is the MLE of the specific time series (i.e., the one which was used to find the RP). In the case of the 100-km fiber link, after training the network using a 100-vector set and their expected outputs (20 vectors for each class), 30 new vectors were tested. The ability of the network to correctly classify the input vector to the correct optical launched power is shown in Fig. 10. The multilayer perceptron perfectly identified the signals launched with 5, 10, 12 and 16 dBm (classes 1, 2, 3 and 5). For the signals launched with 14 dBm, the neural network leads to an uncorrected identification by classing 5 vectors from 30 test vectors as belonging to the category of the 12-dBm launched power. Note, however, that the erroneous launched power estimation keeps the signal within the correct propagation regime identification. In comparison to the cross-correlation stand-alone stage where 20 time series are needed for the identification, the classification stage requires only 5 time-series samples for a correct launched power identification. More sophisticated neural networks based on a decomposition method,¹⁸ for example, can be used to improve the results.

7 Conclusion

We showed that the initial chaotic characteristics of an optical signal are affected by the linear and nonlinear effects

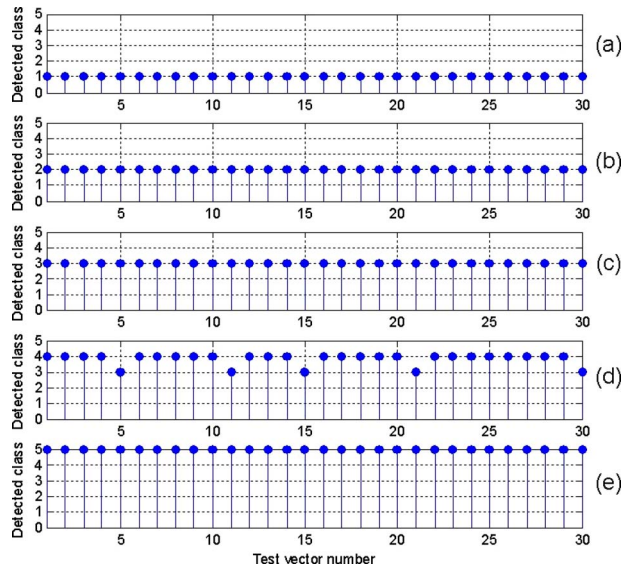


Fig. 10 Classification results using a two-layer multilayer perceptron with 30 test vectors corresponding to time-series signals with launched power of (a) 5, (b) 10, (c) 12, (d) 14, and (e) 16 dBm.

in the optical fiber. The optical launched power changed the properties of the original signal attractor through the nonlinear fiber effects and their interaction with chromatic dispersion.

A set of experiments of a single-channel propagation at 10 Gbps in a 100-km link were been performed and confirmed by numerical simulations. We analyzed the largest Lyapunov exponent value and the RP derived from the signal attractors in the context of the separation between different levels of nonlinearity in an optical signal. It was shown that a multilayer neural network using the MLE, together with the pattern recognition of the RP derived from the attractor, can be used as a classification criterion for identifying the propagation regime of the optical signal and gives a precise evaluation of the signal launched power.

The proposed method based on chaos analysis provides an interesting novel approach for signal propagation regime identification and can be used as monitoring technique in optical links.

Further works will be performed to extend this approach to multiwavelength link transmission.

Appendix: Chaos and Time Series Analysis

The following section provides essential background knowledge on time-series analysis applied to chaos theory for the purpose of the optical propagation regime identification in optical networks.

A.1 Phase Space Reconstruction

The first step in analyzing a nonlinear system from time-series data is to reconstruct an appropriate phase space for the system. The phase space of a system can be reconstructed from the scalar time series of the sampled optical signal, by using the delay-embedding theorem.⁸ This theorem states that one can reconstruct an appropriate phase space using only the original time series and its time-delayed copies, as we recall from Eq. (1):

$$\mathbf{X}_i = \{x_i, x_{i+\tau}, x_{i+2\tau}, \dots, x_{i+(m-1)\tau}\} \quad i = 1, 2, \dots, L, \quad (1')$$

where \mathbf{X}_i is the m -dimensional state vector (known also as attractor⁸), x_i is the original sampled data (the detected optical data), τ is the time delay between copies, and m is the embedding dimension with $L=N-(m-1)\tau$. Appropriate values for τ and m can be obtained with several methods.^{15,19}

In this paper, the method used to determine the sufficient embedding dimension m is based on the chaotic attractor property that its orbits in the phase space should not intersect or overlap with each other.¹⁹ Such an intersection or overlap may result when the attractor is embedded in a dimension lower than the sufficient one stated by the delay-embedding theorem.⁸ An algorithm that makes use of this property to estimate the sufficient dimension m for phase space reconstruction is developed in Ref. 19. This algorithm involves the nearest neighbor search (NNS), which is an optimization problem for finding closest points in metric spaces. Given a set S of points in a metric space M and a query point $q \in M$, the NNS enables to find the closest point in S to q . In many cases, M is taken to be a Euclidean space and distance is measured by Euclidean distance. In our case, the nearest neighbor x_j has to be found for each point x_i in a time-delay embedding m , denote by $R_i(m)$ given in Eq. (3):

$$R_i(m) = \left[\sum_{n=0}^{m-1} (x_{i-n} - x_{i-n})^2 \right]^{1/2}. \quad (3)$$

This calculation is repeated to derive $R_i(m+1)$ in an embedding space $(m+1)$. If $R_i(m+1) > R_i(m)$, then the neighboring points are closed only because of the overlap due to the lack of dimension and are not consider neighbors (false). Thus, the criterion for false nearest neighbors is defined by

$$\frac{|x_{i-m} - x_{i-m}|}{R_i(m)} > R_T, \quad (4)$$

where R_T is a threshold value according to Ref. 15. It is essential to choose optimally the second parameter τ , which is the time delay shift between the time-delayed copies of x_i . A nonoptimal τ yields an attractor that is not adequate to be used for calculating MLE. To find τ , we must to carry out a weak correlation between the delayed copies, which conserves a small statistical dependency.¹⁵ Two main basic approaches are widely used to calculate τ . In the first approach, the first zero crossing of the x_i autocorrelation function is used to yield phase space coordinates that are linearly independent. However, this approach does not always adequately capture nonlinear correlations within the data.¹⁵ Thus, somewhat related but more widely used approach is to choose τ from the first minimum of the AMI function, which evaluates the amount of information I , shared between two data sets over a range of time delays.¹⁵ Equation (5) introduces the average mutual information between two data sets X and Y :

$$\begin{aligned}
 I(X;Y) &= \sum_{i=1}^n \sum_{j=1}^m P(x_i, y_j) I(x_i, y_j) \\
 &= \sum_{i=1}^n \sum_{j=1}^m P(x_i, y_j) \log \frac{P(x_i, y_j)}{P(x_i)P(y_j)}. \quad (5)
 \end{aligned}$$

As we deal with a shifted version of the single data set x_i and $x_{i+\tau}$ Eq. (4) can be written as

$$I(\tau) = \sum_{ij} P_{ij}(\tau) \log P_{ij}(\tau) - 2 \sum_i P_i(\tau), \quad (6)$$

where P_i denotes the probability that x_i takes a value inside the i 'th bin of a histogram, and P_{ij} is the probability that x_i is in the bin i where $x_{i+\tau}$ is in the bin j . The first minimum in the AMI graph is considered as the most suitable choice for τ , since this is the time when $x_{i+\tau}$ adds maximum information to the knowledge we have from x_i .

Currently, determining the proper delay time is still an open problem.¹⁶ There is no common agreement on which of the two methods should be used to determine the delay time. In Ref. 15, there is recommendation to use the first zero crossing of the autocorrelation function on the grounds that it takes into account only linear correlations of the data. On the other hand, the estimation of τ using AMI is reliable only for 2-D embeddings, as mentioned in Ref. 20.

In most practical applications, both methods are employed and it is found either that the estimated delay times are similar or that the two methods yield significantly different values of τ , in which case additional constraints may be needed, such as the construction of 2-D or 3-D phase space for different values of τ to make the final decision.

A.2 Noise Reduction

In general, any sampled signal consists of unavoidable noise. In nonlinear systems, the important parts of the signal often cover the entire spectrum, making signal separation from the noise a difficult task. Signals from chaotic systems exhibit broadband behavior. Therefore, eliminating the noise by using a low-pass filter is impractical.

In this paper, the state space averaging technique^{21,22} is used for noise reduction via prediction. This prediction method separates the deterministic and random components of the time series, since only the deterministic part is predictable. If the deterministic part is the signal and the random part is the noise, a new time-noise-reduced series is constructed. Practically, the separation is never perfect, and removing the noise always distorts the signal to some extent.

The behavior of the chaotic signal can be defined as a clear contour in the phase space with the noise separated from this contour by using a filtering process.²¹ This method looks for points in the time-delayed phase space that are close to the present point to see how they evolve.²² The idea behind this method is that using a future data, a backward prediction can be done. The method described in Ref. 23, considers a window containing $2n$ points around a given point in the m -dimensional phase space denoted $x^{(m)}$, and proceeds to average over a cluster of neighbor points. Every point in the phase space is weighted by $\exp(-d^2/\sigma_N^2)$, where d is distance of each point in the m -dimensional

embedding space from the last known value $x_i^{(m)}$, and σ_N^2 is the standard deviation of the noise. Equations (7) and (8) define the new predicted value of $x^{(m)}$. In general, σ_N^2 is unknown and the results are sensitive to the chosen value and should be optimized for each data set.

$$\bar{x}_i = \frac{\sum_{k=n}^{N-n} w_i(k) x_i}{\sum_{k=n}^{N-n} w_i(k)}, \quad (7)$$

where

$$w_i(k) = \exp \left[-\frac{1}{\sigma_N^2} \sum_{j=-n}^n (x_{k-j} - x_{i-j})^2 \right]. \quad (8)$$

A.3 Largest Lyapunov Exponent

Chaotic systems in general exhibit sensitive dependence on initial conditions, therefore in the phase space, trajectories (orbits), which start arbitrarily near each other, separate exponentially fast. A well-known approach in the chaos theory to measure the chaos degree is given by Lyapunov exponents,²² which provide a direct measure of the sensitive dependence on initial conditions by quantifying the exponential rates at which neighboring orbits on an attractor diverge (or converge) as the system evolves in time. Following the method given in Ref. 9, the MLE is calculated from the sampled optical data signals. According to this method, the Euclidean distances (separation) between each point $x(n)$ and its nearest point $x(l)$ are calculated in the m -dimensional time-delay embedding phase space and we average the logarithmic rate of these separation according to

$$L(k) = \frac{1}{2(N-k-m+1)} \sum_{n=m}^{N-k} \log \sum_{j=0}^{m-1} [x(l-j+k) - x(n-j+k)]^2. \quad (9)$$

The result $L(k)$ is defined as the stretching factor.⁹ The stretching factor $L(k)$ versus k yields a linear increase at the lower k 's, followed by a flat asymptotic. This linear part of the curve represents the exponential increase of $L(k)$ as more points from the orbit are included, while the flat asymptotic region signifies the saturation effect of exponential divergence due to the finite size of the attractor. The largest Lyapunov exponent (λ_1) is given by Eq. (10) at intermediate values of k (i.e., a least-squares line fit for the slope of the first part of the curve).

$$\lambda_1 = dL(k)/dk. \quad (10)$$

A.4 RP

Another measure¹¹ for analyzing chaos systems is by providing a 2-D image, the RP, derived from the matrix distances between all points in the phase space related to the attractor, as

$$R(i,j) := \Theta(\varepsilon - \|\mathbf{X}_i - \mathbf{X}_j\|), \quad (11)$$

where $i, j = 1, \dots, N$. Eq. (11), $\|\cdot\|$ stands for a norm function (e.g., the Euclidean norm), and $\Theta(x)$ is the Heaviside step function. The cutoff distance ε defines a sphere centered at \mathbf{X}_i . When \mathbf{X}_j falls within this sphere, the state will be close to \mathbf{X}_i and thus $R(i,j) = 1$.

Thus, if the point $R(i,j)$ is marked as recurrent, the state j belongs to the neighborhood centered in i of size ε ; this means that the state of the system at time i has some similarity to the state of the system at j : the system is remaining on nearby orbits. The binary values in $R(i,j)$ can be simply visualized by a matrix plot of black and white pixels.

For a stationary signal (e.g., white noise) the dependence should be only on the distance between i and j but not on their position, so that recurrence plot should appear homogeneous. Vertical or horizontal lines on a recurrence plot denote that the system state does not change or changes very slowly in time. Diagonal lines correspond to trajectories passing in the same region as the phase space at different times. Therefore, parallel and perpendicular lines to the main diagonal appear when the series presents some determinism or periodicity. The length of lines parallel to the main diagonal of the recurrence plot indicates how fast the trajectories diverge in phase space. In pure stochastic systems, no parallel or vertical lines appear on a recurrence plot, as in the case of white noise signals. In general, an aggregation of points indicates persistent nonstationary; black bands or areas indicate rare or extreme events.

Acknowledgments

This work was partially supported by the EC-FP7—DICONET (<http://www.diconet.eu>) project. The authors thank Avi Levy from ECI Telecom for providing the OSNR measurements and the different sets of time-series data samples.

References

1. D. C. Kilper, R. Bach, D. J. Blumenthal, D. Einstein, T. Landolsi, L. Ostar, M. Preiss, and A. E. Willner, "Optical performance monitoring," *J. Lightwave Technol.* **22**, 294–304 (2004).
2. D. Pennincks and C. Perret, "New physical analysis of 10-Gb/s transparent optical networks," *IEEE Photonics Technol. Lett.* **15**, 778–780 (2003).
3. X. Wu, J. Jargon, L. Christen, and A. Willner, "Training of neural networks to perform optical performance monitoring of a combination of accumulated signal nonlinearity, CD, PMD and OSNR," in *Proc. LEOS 2008*, 543–549 (2008).
4. J. Mørk, B. Tromborg, and J. Mark, "Chaos in semiconductor lasers with optical feedback: Theory and experiment," *IEEE J. Quantum Electron.* **28**, 93–108 (1992).
5. J. M. Liu, H. F. Chen, and S. Tang, "Synchronized chaotic optical communications at high bit rates," *IEEE J. Quantum Electron.* **38**, 1184–1196 (2002).
6. W. L. Zhang, W. Pan, B. Luo, X. H. Zou, and M. Y. Wang, "One-to-many and many-to-one optical chaos communications using semiconductor lasers," *IEEE Photonics Technol. Lett.* **20**, 712–714 (2008).
7. N. H. Packard, J. P. Crutchfield, J. D. Farmer, and R. Shaw, "Geometry from a time series," *Phys. Rev. Lett.* **45**, 712–716 (1980).
8. F. Takens, "Detecting strange attractors in turbulence," in *Dynamic systems and turbulence, Warwick, 1980*, D. A. Rand and L. S. Young, Eds., pp. 366–381, Springer Verlag, Coventry, England (1981).
9. M. T. Rosenstein, J. J. Collins, and C. J. de Luca, "A practical method for calculating largest Lyapunov exponents from small data sets," *Physica D* **65**, 117–134 (1993).
10. M. Norbert, W. Niels, M. Udo, S. Alexander, and K. Jurgen, "Recurrence-plot-based measures of complexity and their application to heart-rate-variability data," *Phys. Rev. E* **66**, 026702 (2002).
11. U. Mahlab and J. Shamir, "Genetic algorithm for optical pattern recognition," *Opt. Lett.* **16**, 648–650 (1991).
12. U. Mahlab and J. Shamir, "Optical pattern recognition based on convex function," *J. Opt. Soc. Am. A* **8**, 1233–1239 (1991).
13. U. Mahlab and J. Shamir, "Phase only entropy filter generated by simulated annealing," *Opt. Lett.* **14**, 1168–1170 (1989).
14. G. P. Agrawal, *Nonlinear Fiber Optics*, 3rd ed., Academic Press, San Diego (2001).
15. H. D. I. Abarbanel, *Analysis of Observed Chaotic Data*, Springer-Verlag (1996).
16. A. M. Albano, A. Passamante, and M. E. Farrell, "Using higher-order correlations to define an embedding window," *Physica D* **54**, 85–97 (1991).
17. K. Mehrotra, C. K. Mohan, and S. Ranka, *Elements of Artificial Neural Networks* MIT Press, Boston, MA (1997).
18. H. El Ayeche and A. Trabelsi, "Decomposition method for neural multiclass classification problem," *Proc. World Acad. Sci. Eng. Technol.* **15**, 151–153 (2006).
19. M. B. Kennel, R. Brown, and H. D. I. Abarbanel, "Determining minimum embedding dimension using a geometric construction," *Phys. Rev. A* **23**, 3403–3411 (1992).
20. H. Kantz and T. Schreiber, *Nonlinear Time Series Analysis*, Cambridge University Press, Cambridge, UK (1996).
21. T. Schreiber, "Extremely simple nonlinear noise reduction method," *Phys. Rev. E* **47**, 2401–2404 (1993).
22. J. C. Sprott, *Chaos and Time-Series Analysis*, Oxford University Press, New York (2003).
23. R. Hegger, H. Kantz, and T. Schreiber, "Practical implementation of nonlinear time series method: the TISEAN package," *Chaos* **9**, 413–435 (1999).



Rony Rahamim received his engineer's diploma in electrical and electronics engineering from Coventry University, in collaboration with Ruppim College, Israel, in 2000 and his MSc degree in electrical engineering from the Holon Academic Institute of Technology (HIT), Israel, in 2008. In 2000, he joined ECI Telecom and has been involved in the field of broadband access solutions, developing line-cards-based example digital subscriber line (xDSL) and voice over IP (Internet protocol) technology. His research interests include chaos, application of chaos to security information, and chaotic time series analysis for optical networks.



Uri Mahlab received his BSc degree in electrical engineering from the Ben Gurion University of the Negev, Beer-Sheva, Israel, and his MSc and PhD degrees in electrical engineering from the Technion-Israel Institute of Technology, Haifa, in 1989 and 1992, respectively. Dr. Mahlab is a senior lecturer with the Holon Academic Institute of Technology (HIT) in Holon, Israel, in the Electrical Engineering Department and has been a member of HIT since 1994. He has been involved in industry since 1992. He was with the electro-optical industry in Israel (ELOP), with the Tadiran Co. in the field of military communication, and since 1998 with ECI Telecom in the Networks Solution Division, in the field of optical technologies and networking. He has initiated and participated in several research programs in optical fiber communications, and has been involved in the European Consortium under the IST activity FP5 and FP7 programs in the Metropolitan Terabit Optical Ring (METEOR) and the Dynamic Impairment Constraint Network for Transparent Mesh Optical Networks (DICONET) projects and in four research projects related to optical networks since 2002 funded by the Israeli Ministry of Science. He is a member of OSA and a senior member of IEEE.



David Dahan received his engineer's diploma in electrical engineering from Supélec, France, in 1999, his MSc degree in electrical and computer engineering from the Georgia Institute of Technology in 1999, and his PhD degree in electrical engineering from the Technion-Israel Institute of Technology in 2006. In 2007, he joined ECI Telecom, in the field of optical technologies and networking, and he has been involved in the European consortium under the IST activity FP7 programs in the Dynamic Impairment Constraint Network for Transparent Mesh Optical Networks (DICONET) project,

and the Digital and Analog Advanced Modulation Formats for high-capacity Optical Network Deployment (DiAMOND) project, partially funded by the Israeli Ministry of Science. His research interests include advanced optical modulation formats, optical performance and impairment monitoring techniques, slow and fast light in optical fibers, wavelength converters and reshapers, optical pulse generation, and self-starting optoelectronic oscillators. He is an author and coauthor of more than 35 journal and conference papers and a reviewer for several international peer-reviewed journals. He received a fellowship of excellence from the Israel Ministry of Science from 2003 to 2005 and the IEEE/LEOS graduate student fellowship award in 2004. He is a member of the IEEE/LEOS Society.